Origins of abnormal behaviors of gelatinous layer in tension wood fiber - A micromechanical approach

Hiroyuki Yamamoto, Julien Ruelle, Yoshiharu Arakawa, Masato Yoshida, Bruno Clair, Joseph Gril

Origins of abnormal behaviors of gelatinous layer in tension wood fiber - A micromechanical approach

H. Yamamoto[1], J. Ruelle[2], Y. Arakawa[1], M. Yoshida[1], B. Clair[2] and J. Gril[2]

[1] Nagoya University, Japan; [2] Université Montpellier 2, France

Abstract

The mechanism responsible for unusual mechanical properties of tension wood gelatinous fiber (G-fiber) was investigated. We discussed origins of high tensile growth stress, high drying shrinkage, and rapid increase of Young's modulus due to drying, in association with microscopic structure of gelatinous layer (G-layer). Anatomical, crystallographic, and micromechanical approaches were employed. As the result, it is cleared that G-layer structure as hydro-gel has a key to understand hygromechanical properties in the tension wood G-fiber. The origin of contractive force in maturing G-layer is still unknown, however, the structure and behavior of the swollen hydro-gel may give some key to solve it.

Introduction

Tension wood xylem often produces an unusual wood fiber known as gelatinous fiber (G-fiber) along the upper sides of leaning stems or branches in woody eudicot species. The G-fibers form a gelatinous layer (G-layer) as the innermost layer of the multilayered cell wall, characterized by the absence of lignin and a high concentration of rigid cellulose microfibrils aligned along the fiber axis (see *Fig.1*) [1](Onaka 1949).

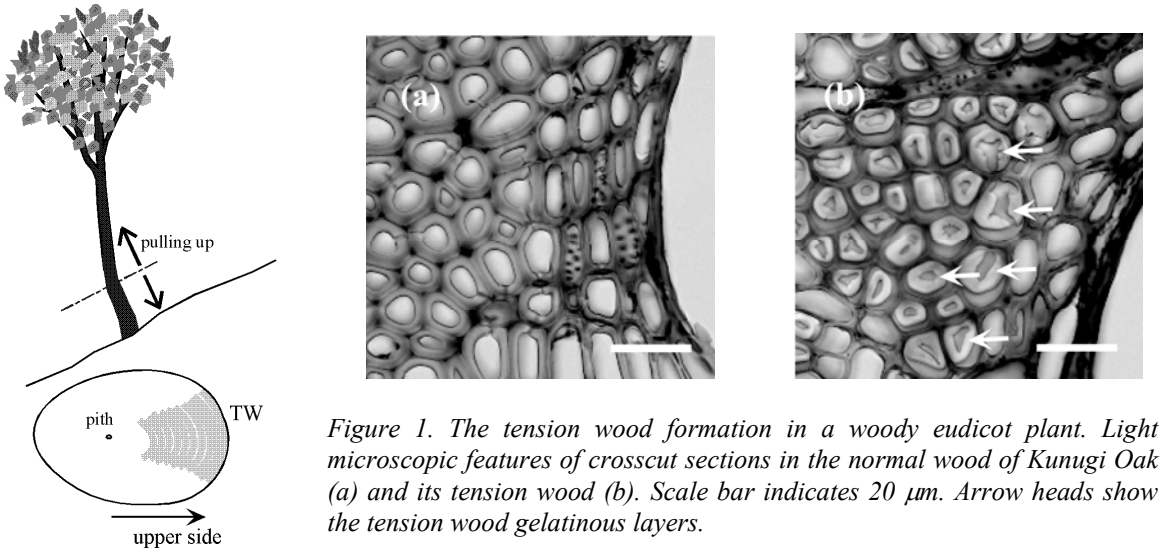

Figure 1. The tension wood formation in a woody eudicot plant. Light microscopic features of crosscut sections in the normal wood of Kunugi Oak (a) and its tension wood (b). Scale bar indicates 20 μm. Arrow heads show the tension wood gelatinous layers.

G-fibers generate high tensile growth stress during the maturation process [2-12], which enables hardwood species to perform negative-gravitropic behavior in inclined shoots [13-15]. However, in timber production, tension wood is often the source of various problems, such as processing defects caused by its abnormal growth stress [16,17]. Other particularities are a high longitudinal Young's

modulus and a high longitudinal drying shrinkage [4,6,8,18], the combined effect of which cause serious complications during the drying process, such as distortion and longitudinal cleavage of the sawn lumber.

Some studies have suggested that the distinctive properties of G-fibers could be attributed to the intrinsic behavior of the G-layer [2,3,11,4,6,19,8,9], while others have emphasized the role of the lignified layer (L-layer), which often peels off the G-layer along the same direction during microtoming [20,21,22]. Recently, Clair et al. [23] noted that detachment of the G-layer, often observed in the microtomed surface of a fresh block, disappeared at a distance greater than 100 μm from the block surface, which was embedded in resin after being oven-dried. This finding supports the view that the intrinsic property of the G-layer is the source of the characteristic behavior of G-fibers. However, the generation mechanism of the G-layer properties is still unknown. In the present study, we focused on generation of the abnormal tensile growth stress, and moisture-dependent changes in the longitudinal Young's modulus and longitudinal shrinkage in tension wood of two Kunugi oak (*Quercus acutissima*) trees, revealing the property difference between the G-layer and L-layer.

Material and methods

Sampled trees

The studied specimens were two Kunugi oaks (*Quercus acutissima*), a 75-year-old tree (Kunugi A) and a 40-year-old tree (Kunugi B), grown in Nagoya, Japan. The girths at chest height were 103 cm (Kunugi A) and 73 cm (Kunugi B); both trees had inclined stems.

Measurement of the released strain of the surface growth stress (ε_L)

At the chest height, 10 or 11 points were set around the circumference of each stem. Released strain of the surface growth stress (ε_L) was measured at each point, using the strain-gauge method. Measurement was done in December 2002.

Measurements of longitudinal Young's modulus (E_L)

Thin blocks were prepared from each measuring point of the released strain, and were cut for the tensile and shrinkage tests at the macroscopic level, with specimen size 70 (Longitudinal, L) × 10 (Tangential, T) × 4 (Radial, R) and 50 (L) × 13 (T) × 5 (R) mm^3, respectively.

Tensile tests at the macroscopic level were performed in green and oven-dried conditions at the temperature controlled room (20 ˚C). For each specimen, two strain gauges were bonded at the center of the flat-sawn surfaces and connected to the strain-meter. Tensile test was performed by using a commercial equipment. The outputs from both strain-gauges were collected and averaged. And, the macroscopic longitudinal Young's modulus (E_L) was determined from the stress–strain curve.

Measurements of longitudinal drying shrinkage (α_L)

A hand-made comparator with a high precision dial gauge (0.001 mm in accuracy) was employed for the measurement of the dimension of the specimen [4,24]. Thus, macroscopic oven-dried shrinkage (α_L) was calculated as

$$\alpha_L = (l_{wet} - l_{dry})/l_{wet} \times 100 \quad (\%) \qquad (1)$$

where l_{wet} and l_{dry} are the longitudinal dimensions of the macroscopic specimen at the green condition and under the oven-dried condition, respectively.

X-ray diffraction properties of cell wall cellulose

Specimen:

From both the heavy tension and opposite wood (normal wood) sides in Kunugi A, a sample block was taken, and two types of specimen were prepared, flat-sawn sections [15 (L) × 10 (T) × 0.2 (R) mm] and coarse sawdust powder. For the flat-sawn sections, eight specimens were prepared from extra-porous zones in the wood blocks. For the sawdust powders, sufficient amounts of powder were prepared, and they were fully stirred to become uniform. Those samples were seasoned inside a small air-conditioned desiccator with water until equilibrium so as to remove liquid water that remarkably increases a halo peak in the X-ray diffraction diagram. The powder sample was packed into the plate-like specimen holder before seasoning. The moisture condition of the samples in this stage was regarded as the fiber saturation point (FSP), and we used them for diffraction analysis at the FSP with the reflection technique using a X-ray diffractometer. Samples were then air-dried until equilibrium and X-ray measurements retaken, followed by oven-drying for 24 h at 105 °C after seasoning inside a desiccator with a powder of P_2O_5 and further measurements retaken [25].

Measurements of width of a single crystallite (WSC) and lattice distance from [200] plane (d_{200}):

CuKα was used as a line-focused incident X-ray with a power of 35 kV, 35 mA, and passed through a Ni filter. For flat-sawn sections, diffraction intensity was recorded in the 2θ angular range from 5º to 40º to determine the half width of the [200] diffraction peak (β) that was transformed into width of a single fibrous crystallite (*WSC*) in a direction perpendicular to the [200] plane. In addition, the diffraction intensities from the powder samples were recorded in the 2θ angular range from 20º to 25º to determine the peak angle from the [200] lattice plane ($2\theta_{200}$) under the various moisture condition. In this measurement, three powder samples were prepared for each of tension wood and normal wood, while one sample for isolated G-layer powder that was prepared from a heavy tension wood block using the technique described by Norberg and Meier [20].

The *WSC* value was estimated from flat-sawn sections based on the study of Hengstenberg et al. [26] using the modified Scherrer's equation:

$$WSC = K \cdot \lambda / (\beta \cdot \cos\theta_{200}) \quad \text{(nm)} \tag{2}$$

where K is a constant (The present study assumed $K = 1$), λ is the wavelength of CuKα (= 0.154 nm), β is the half-width of the [200] diffraction peak, and θ_{200} is the peak position from the [200] plane.

The value of d_{200} was determined from powder samples based on Bragg's equation:

$$d_{200} = \lambda / (2\sin\theta_{200}) \quad \text{(nm)} \tag{3}$$

Histo-mechanical approach for modeling

After the Young's modulus and drying shrinkage measurements, a small block was sampled from each specimen. A transverse section was cut from each block on a sliding microtome and microscopic images at high and low magnification were recorded within the outermost annual rings of the mounted section under a light microscope connected to an image processor. Macroscopic xylem consists of vessel elements including the vasicentric parenchymae (*V*), ray parenchymae (*R*), and wood fiber (*F*). From the low magnification images, the areal composition of each domain in cross section was computed. The areal ratio of the G-fiber in the domain of wood fiber (ϕ) was also measured. From high magnification images, the ratios of the G-layer (g), L-layer (l), and total cell wall (w) areas in the domain of wood fiber were determined. Moreover, the areal ratios of the G-layer (γ) and L-layer (λ) in wood-fiber cell wall were also calculated. The relationships between the anatomical parameters were as follows: $V + R + F = 1$, $g + l = w$, and $\gamma + \lambda = 1$.

The simple law of mixture gives the following formulae to estimate growth strain (ε_L^F), Young's modulus (E_L^F), and drying shrinkage (α_L^F) of the wood-fiber domain along the fiber axis in each specimen [6]:

$$\varepsilon_L^F \cong \varepsilon_L, \quad E_L^F \cong E_L / F, \quad \text{and} \quad \alpha_L^F \cong \alpha_L \tag{4}$$

assuming that the vessel and ray tissues are not involved in determining the axial growth strain, elasticity and shrinkage of the xylem.

The wood-fiber domain is composed of two types of slender, thick-walled fibers—gelatinous (G-fiber) and normal fibers (N-fiber)—arranged in rows in a direction parallel to the wood-fiber axis. In previous works by Clair et al. [8] and Yamamoto et al. [6], the simple law of mixture was applied to relate the longitudinal properties in a macroscopic wood with fiber properties. We then used the following equations:

$$\varepsilon_{\mathrm{L}}^{\mathrm{F}}\left(\cong \varepsilon_{\mathrm{L}}\right)= \frac{\phi \cdot E_{\mathrm{L}}^{\mathrm{g}} \cdot \varepsilon_{\mathrm{L}}^{\mathrm{g}} + (1-\phi)\cdot E_{\mathrm{L}}^{\mathrm{n}} \cdot \varepsilon_{\mathrm{L}}^{\mathrm{n}}}{\phi \cdot E_{\mathrm{L}}^{\mathrm{g}} + (1-\phi) E_{\mathrm{L}}^{\mathrm{n}}} \quad , \quad E_{\mathrm{L}}^{\mathrm{F}} = \phi \cdot E_{\mathrm{L}}^{\mathrm{g}} + (1-\phi) E_{\mathrm{L}}^{\mathrm{n}} \quad ,$$

$$\alpha_{\mathrm{L}}^{\mathrm{F}}\left(\cong \alpha_{\mathrm{L}}\right)= \frac{\phi \cdot E_{\mathrm{L}}^{\mathrm{g}} \cdot \alpha_{\mathrm{L}}^{\mathrm{g}} + (1-\phi)\cdot E_{\mathrm{L}}^{\mathrm{n}} \cdot \alpha_{\mathrm{L}}^{\mathrm{n}}}{\phi \cdot E_{\mathrm{L}}^{\mathrm{g}} + (1-\phi) E_{\mathrm{L}}^{\mathrm{n}}} \quad , \tag{5}$$

where $\varepsilon_{\mathrm{L}}^{\mathrm{g}}$ and $\varepsilon_{\mathrm{L}}^{\mathrm{n}}$ are the growth strains of the G- and N-fiber, respectively, and $E_{\mathrm{L}}^{\mathrm{g}}$ and $E_{\mathrm{L}}^{\mathrm{n}}$ are their respective Young's modulus, and $\alpha_{\mathrm{L}}^{\mathrm{g}}$ and $\alpha_{\mathrm{L}}^{\mathrm{n}}$ are drying shrinkages in respective fibers.

The cell wall of the wood fiber consists of G- and L-layers, which are also arranged in rows parallel to the wood-fiber axis. The simple law of mixture now gives the following equations:

$$\varepsilon_{\mathrm{L}}^{\mathrm{W}}(\cong \varepsilon_{\mathrm{L}})= \frac{\gamma \cdot E^{\mathrm{G}} \cdot \varepsilon^{\mathrm{G}} + (1-\gamma)\cdot E^{\mathrm{S}} \cdot \varepsilon^{\mathrm{S}}}{\gamma \cdot E^{\mathrm{G}} + (1-\gamma)\cdot E^{\mathrm{S}}} \quad , \quad E_{\mathrm{L}}^{\mathrm{W}} = \gamma \cdot E^{\mathrm{G}} + (1-\gamma) E^{\mathrm{S}} \quad ,$$

$$\alpha_{\mathrm{L}}^{\mathrm{W}}(\cong \alpha_{\mathrm{L}})= \frac{\gamma \cdot E^{\mathrm{G}} \cdot \alpha^{\mathrm{G}} + (1-\gamma)\cdot E^{\mathrm{S}} \cdot \alpha^{\mathrm{S}}}{\gamma \cdot E^{\mathrm{G}} + (1-\gamma)\cdot E^{\mathrm{S}}} \quad , \tag{6}$$

where $\varepsilon_{\mathrm{L}}^{\mathrm{W}}$ is the growth strains, and $E_{\mathrm{L}}^{\mathrm{W}}$ (= $E_{\mathrm{L}}^{\mathrm{F}}/w$) is the substantial Young's modulus, and $\alpha_{\mathrm{L}}^{\mathrm{W}}$ ($\approx \alpha_{\mathrm{L}}^{\mathrm{F}}$) is the drying shrinkage of the cell wall in the direction parallel to the fiber axis. ε^{G} and ε^{S} are the growth strains of the G- and L-layer, respectively, and E^{G} and E^{S} are the Young's modulus of the G-layer along the direction of the fiber and that of the L-layer, respectively, and α^{G} and α^{S} are their respective shrinkages.

The values of $E_{\mathrm{L}}^{\mathrm{g}}$ and $E_{\mathrm{L}}^{\mathrm{n}}$ in the green and the oven-dried specimen were optimized by applying the least square method using the second formula of (5) to the observed relationship between $E_{\mathrm{L}}^{\mathrm{F}}$ and ϕ. After that, the values of $\varepsilon_{\mathrm{L}}^{\mathrm{g}}$, $\varepsilon_{\mathrm{L}}^{\mathrm{n}}$ were determined from the observed relationship between $\varepsilon_{\mathrm{L}}^{\mathrm{F}}$ and ϕ. When determining the values of $\varepsilon_{\mathrm{L}}^{\mathrm{g}}$ and $\varepsilon_{\mathrm{L}}^{\mathrm{n}}$ using the first formula of (5), we adopted the determined values of $E_{\mathrm{L}}^{\mathrm{g}}$ and $E_{\mathrm{L}}^{\mathrm{n}}$ in the green specimen to the calculation. Moreover, the values of $\alpha_{\mathrm{L}}^{\mathrm{g}}$, $\alpha_{\mathrm{L}}^{\mathrm{n}}$, and r (=$E_{\mathrm{L}}^{\mathrm{g}}/ E_{\mathrm{L}}^{\mathrm{n}}$) in the third equation of (5) were also determined from the observed relationship between $\alpha_{\mathrm{L}}^{\mathrm{F}}$ and ϕ. In the same manner as those cases, E^{G}, E^{S}, $\varepsilon_{\mathrm{L}}^{\mathrm{g}}$, $\varepsilon_{\mathrm{L}}^{\mathrm{n}}$, α^{G}, α^{S}, and s (=$E^{\mathrm{G}}/ E^{\mathrm{S}}$) were determined from the observed relations between $E_{\mathrm{L}}^{\mathrm{W}}$, $\varepsilon_{\mathrm{L}}^{\mathrm{W}}$, $\alpha_{\mathrm{L}}^{\mathrm{W}}$ and γ through the least square method using equations (6).

Results

Young's moduli of the fibers and layers

Estimated values of $E_{\mathrm{L}}^{\mathrm{g}}$, $E_{\mathrm{L}}^{\mathrm{n}}$, E^{G}, and E^{S} are displayed in Table 1. The values of $E_{\mathrm{L}}^{\mathrm{g}}$ and $E_{\mathrm{L}}^{\mathrm{n}}$ were quite different between two trees. This is because the most of wood fiber has a quite thicker cell wall in Kunugi B than in Kunugi A. After eliminating the effect of cell-wall thickness, those differences became smaller as shown in Table 1.

As a result of drying from green to oven-dried condition, the Young's modulus in L-layer (E^{S}) increased by 22.1% in Kunugi A and 29.7% in Kunugi B. Those values are in close agreement with values reported previously for Spruce [27] and Japanese cedar [28]. On the other hand, the Young's modulus of G-layer increased considerably with the drying process at a ratio of 204.6% in Kunugi A and 80.4% in Kunugi B.

Growth strain in fibers and layers

The estimated values of growth strains in fibers (= ε_L^g and ε_L^n) and wall layers are displayed in Table 2. It is clearly concluded that contractive growth strain becomes quite higher in the G-layer than in the normal lignified layer, which causes generation of a very large tensile growth stress in the G-fiber.

Drying shrinkage of fibers and layers from green to oven-dried condition

The estimated values of α_L^g, α_L^n, α^G, and α^S were determined as displayed in Table 3. As a result of drying from green to oven-dried condition, each layer contracted in the direction parallel to the fiber axis. On the other hand, the G-layer contracted several times higher than the L-layer in each tree, which causes generation of a very large drying shrinkage in the G-fiber. It is considered that the combined effect of increase in Young's modulus and drying shrinkage along the fiber direction causes serious complications during the drying process, such as distortion, longitudinal cleavage of the sawn lumber, and so forth.

Table 1. Young's moduli of fiber and layer.

	Kunugi A		Kunugi B	
	green	Oven-dried	Green	Oven-dried
Fiber Young's modulus (GPa)				
E_L^s	14.79 (+/- 0.60)	17.70 (+/- 1.61)	22.79 (+/- 1.01)	29.52 (+/- 1.61)
E_L^g	15.98 (+/- 0.84)	39.61 (+/- 2.26)	25.02 (+/- 1.40)	41.64 (+/- 2.23)
Layer Young's modulus (GPa)				
E^S	19.49 (+/- 1.04)	23.79 (+/- 2.50)	24.86 (+/- 1.51)	32.24 (+/- 1.96)
E^G	27.88 (+/- 9.94)	84.92 (+/- 7.40)	38.10 (+/- 4.02)	68.73 (+/- 5.22)

Parenses stand for +/− 95 % confidence interval of the mean value.

Table 2. Growth strains in fiber and layer.

	Kunugi A	Kunugi B
Fiber growth strain (%)		
ε_L^s	-0.0167 (+/- 0.0051)	-0.0334 (+/- 0.0056)
ε_L^g	-0.3222 (+/- 0.0182)	-0.2499 (+/- 0.0322)
Layer growth strain (%)		
ε^S	-0.0192 (+/- 0.0041)	-0.0334 (+/- 0.0091)
ε^G	-0.4625 (+/- 0.0389)	-0.3206 (+/- 0.0552)

Parenses stand for +/− 95 % confidence interval of the mean value.

Table 3. Drying shrinkage in fiber and layer.

	Kunugi A	Kunugi B
Fiber shrinkage (%)		
α_L^s	0.294 (+/- 0.083)	0.058 (+/- 0.056)
α_L^g	1.000 (+/- 0. 085)	0.914 (+/- 0.081)
Layer shrinkage (%)		
α^S	0.293 (+/- 0.083)	0.058 (+/- 0.058)
α^G	1.108 (+/- 0.100)	1.122 (+/- 0.108)

Parenses stand for +/− 95 % confidence interval of the mean value.

X-ray diffraction properties in TW cellulose

Figure 1 shows X-ray diffracto-grams of various powder samples under air-dried conditions. The diffractogram of the isolated G-layer (c) was almost identical to that of Avicel powder (a), which suggests that the G-layer contains large amounts of native cellulose crystallites. The diffractogram of normal wood (b) showed a typical pattern of ligno-cellulosic material in which the peak separation between [1$\underline{1}$0] and [110] was unclear. The diffraction of tension wood powder (d) gave a similar pattern as the G-layer (c), which shows that tension wood contains a large number of G-layers.

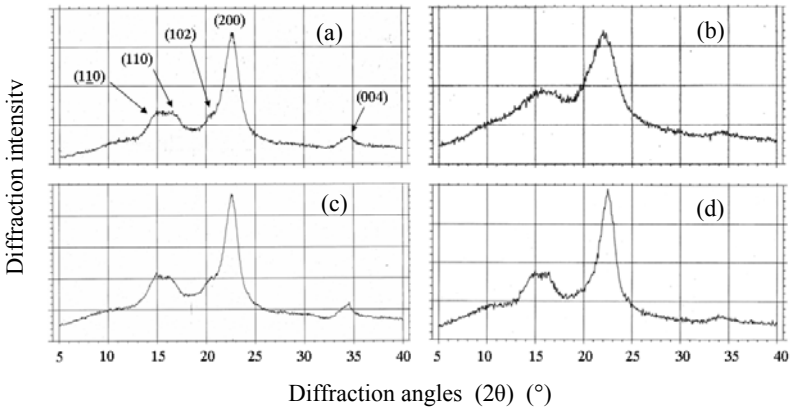

Fig.1. X-ray diffraction patterns from (a) native cellulose powder (Avicell), (b) Kunugi normal wood powder, (c) isolated G-layer powder from Kunugi tension wood, and (d) Kunugi tension wood powder. The measurements were done in the air-dried condition.

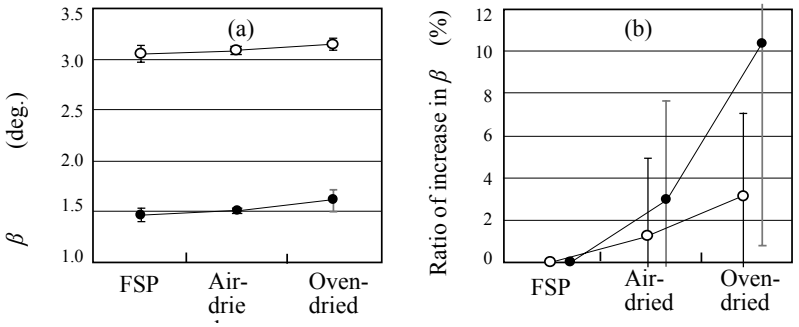

Fig. 2 (a) Half width of [200] peak (β) under various moisture conditions. (b) Changes in the ratio of increase of β, calculated on the basis of β at the FSP. The error bar denotes ± SD of eight samples. Solid circle: tension wood sections; open circle: normal wood sections.

Figure 2(a) shows the half width of the [200] diffraction peak (β) in normal and tension wood sections under various moisture conditions. Figure 2(b) shows the ratios of increase in β calculated on the basis of β at the FSP. The value of β tended to increase with drying, which was noticeably higher in the tension wood than in the normal wood. Figure 3(a) shows values of *WSC*, calculated from equation (2), in normal and tension wood sections under various moisture conditions. Figure 3(b) shows the ratios of increase in *WSC* calculated on the basis of *WSC* at the FSP. Figures 3 indicate that the *WSC*s in the normal and tension wood sections decreased with drying, with the ratio of decrease being higher in the tension wood (9.06%) than in the normal wood (3.05%).

Figure 4(a) shows the lattice distance in the [200] plane (d_{200}) in normal and tension wood powders under various moisture conditions; Fig. 4(b) shows the ratios of increase in d_{200} on the basis of d_{200} at the FSP. The values of d_{200} increased as the drying proceeded, and the ratios of increase from FSP to oven-dry were more or less identical in both wood (1.88 % in the tension wood, and 1.77 % in the normal wood).

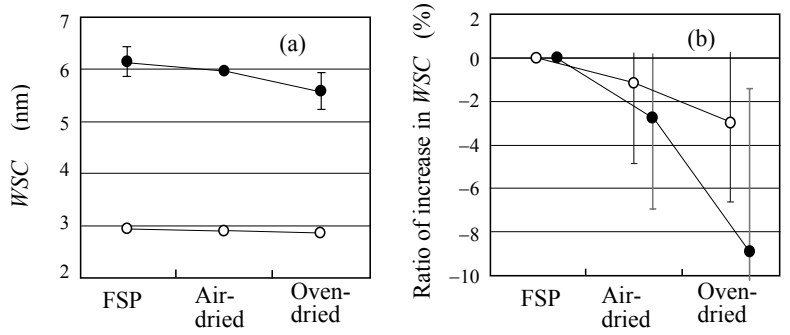

Fig. 3 (a) Width of a single crystallite in the direction perpendicular to the [200] plane (WSC) under various moisture conditions. (b) Changes in the ratio of increase in WSC, calculated on the basis of WSC at the FSP. The error bar denotes ± SD of eight samples. Solid circles: tension wood sections; open circles: normal wood sections.

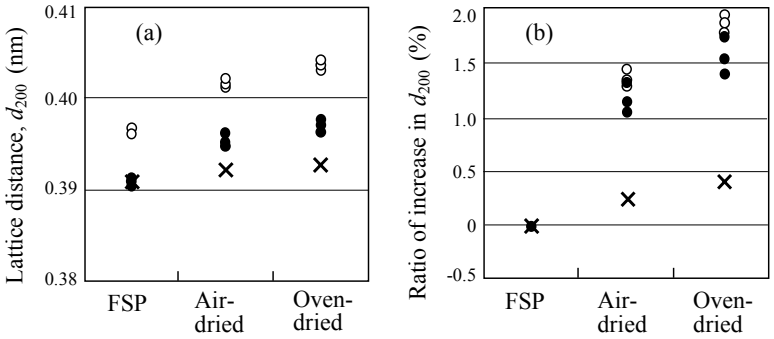

Fig. 4. (a) Lattice distance (d_{200}) of powder samples under various moisture conditions. (b) Ratio of increase in d_{200}, calculated on the basis of d_{200} at the FSP. Solid circles: tension wood powders; open circles: normal wood powders; cross: powder of isolated G-layer.

Discussion

In the present study, we showed that contractive growth strain was larger in the G-layer than in the L-layer, and the ratio of increase in the longitudinal Young's modulus with drying was higher in the G-layer than in the L-layer, a pattern repeated with longitudinal drying shrinkage. Thus, we concluded that the generation of abnormally large tensile stress in the G-layer causes the large tensile growth stress in the tension wood region, and that the increased Young's modulus with drying in the G-layer compared to the L-layer causes the large increase in the Young's modulus of tension wood after drying. We also concluded that an abnormally large shrinkage with drying in the G-layer compared to the L-layer causes the large shrinkage in the drying tension wood.

As reported by Clair et al. [29], transverse sectioning often causes an artefactual swelling in the crosscut shapes of the G-layer, resulting in an overestimation of the values of g and γ. This could lead to an underestimation of the differences in the physical properties between the G-layer and the L-layer. However, we consider that the obtained conclusion is not disturbed by such an artifact because difference of the properties between the G- and the L-layers would be even greater if we took the possible overestimation of g and γ into consideration.

We also discovered that the lattice distance in the [200] plane (d_{200}) increased with drying, while the width of a single crystallite (*WSC*) in the direction perpendicular to the [200] plane became smaller after drying, which is especially noticeably in the tension wood. The latter result comes from the increase in the half width of the [200] diffraction peak (β) with drying. Lately, Clair et al. [30] showed that the tension wood cell wall has a gel-like structure characterized by a pore surface more than 30 times higher by analyzing nitrogen adsorption–desorption isotherms of supercritically dried tension and normal wood. Although the present results seem to be unrelated, the origin of these complex phenomena can be explained in the following manner via the gel-like structure of the tension wood cell wall proposed by Clair et al. [30].

The G-layer matrix consists of a substantial amount of noncrystalline polysaccharides (NCPs), which in the green state, behaves as a water-swollen gel. During water desorption after lumbering, the swollen gel of the NCPs collapses under surface tension. As a result, the matrix is transformed into a condensed structure by strong hydrogen bonding between NCP molecules, which is a form of xero-gelation, leading to an abnormal increase in the Young's modulus and high shrinkage in the drying G-layer. It is considered the NCPs consist of small amount of hemicellulose besides non-crystalline cellulose, e.g., galactan, xyloglucan, and so forth [20,31]. According to Nishikubo et al.[31], most of non-cellulosic polysaccharide consists of xyloglucan, therefore, it is considered that xyloglucan might have something important role to control the mechanical behaviors of G-layer.

Lately, Fang et al. [32] reported that relative thickness of G-layer became significantly smaller than that of the lignified layer after drying; moreover, lumen size in G-fiber increased while that in the N-fiber decreased after drying. Their discovery suggests a possibility that a tensile stress is generated in

the dried G-layer not only in the longitudinal but also circumferential directions. In other word, it is considered that some cellulose microfibrils in the dried G-layer are subject to transverse tensile and longitudinal buckling stresses from the shrinking NCP matrix. The combined effect causes disarray in the cellulose lattice arrangements, especially at the surface layer of each crystallite, which may cause increase of β and thus apparent decrease of *WSC* after drying. This may explain why d_{200} increases while *WSC* decreases in the dried G-layer. The possibility of longitudinal buckling in cellulose crystallites was also noted by Clair et al. [9]. Considering that anisotropic structure of cellulose crystallite, transverse stiffness is relatively lower in the direction perpendicular to the [200] lattice plane than in the direction along b-axis in unit cell, possibly causing each crystallite more easily to deform or delaminate in the direction perpendicular to the [200] lattice plane than in the direction along b-axis under external negative pressure.

In the L-layer matrix, NCP molecules are reinforced by large amounts of lignin whose rigidity is higher than that of the NCPs under the wet condition [33,34]. As with the NCP matrix in the G-layer, the NCP domain in the green, lignified cell wall collapses with moisture desorption; however, its condensation and resulting xero-gelation is mechanically prevented by the lignin, which acts as a rigid skeleton in the matrix [35,36]. Thus, the ratio of increase in the longitudinal Young's modulus with drying is lower in the L-layer than in the G-layer; longitudinal drying shrinkage also displayed a similar pattern of behavior. The increases in β values (and decrease in *WSC*) were thus lower in the L-layer than in the G-layer.

At this time, the mechanism of generation of contractive force in the maturing G-layer is still unknown, however, the structure and behavior of swollen hydro-gel may give some key to solve it.

References

1. Onaka, F. (1949): *Study on reaction wood*. Wood Research (Bull Wood Res Inst Kyoto Univ). 1: 1-99.
2. Okuyama, T., H. Yamamoto, M. Iguchi and M. Yoshida (1990): *Generation process of growth stresses in cell walls. II. Growth stress in tension wood*. Mokuzai Gakkaishi. 36: 797-803.
3. Okuyama, T., H. Yamamoto, M. Yoshida, Y. Hattori and R.R. Archer (1994): *Growth stresses in tension wood. Role of microfibrils and lignification*. Annals Sciences Forestierre. 51: 291-300.
4. Yamamoto, H., T. Okuyama, K. Sugiyama and M. Yoshida (1992): *Generation process of growth stresses in cell walls. IV. Action of the cellulose microfibrils upon the generation of the tensile stresses*. Mokuzai Gakkaishi. 38: 107-113.
5. Yamamoto, H., T. Okuyama and M. Yoshida (1993): *Generation process of growth stresses in cell walls. V. Model of tensile stress generation in gelatinous fibers*. Mokuzai Gakkaishi. 39: 118-125.
6. Yamamoto, H., K. Abe, Y. Arakawa, T. Okuyama and J. Gril (2005): *Role of the gelatinous layer (G-layer) on the origin of the physical properties of the tension wood of Acer sieboldianum*. Journal of Wood Science. 51: 222-233.
7. Yoshida, M., H. Ohta and T. Okuyama (2002): *Tensile growth stress and lignin distribution in the cell walls of black locust (Robinia pseudoacacia)*. Journal of Wood Science. 48: 99-105.
8. Clair, B., J. Ruelle and B. Thibaut (2003): *Relationship between growth stress, mechanical- physical properties and proportion of fibre with gelatinous layer in chestnut (Castanea sativa Mill.)*. Holzforschung 57: 189-195.
9. Clair, B., T. Almeras, H. Yamamoto, T. Okuyama and J. Sugiyama (2006): *Mechanical Behavior of cellulose microfibrils in tension wood, in relation with maturation stress generation*. Biophysics Journal. 91: 1128-1135.
10. Yamamoto, H. (1998): *Generation mechanism of growth stresses in wood cell walls: Roles of lignin deposition and cellulose microfibril during cell wall maturation*. Wood Science and Technology. 32: 171-182.
11. Yamamoto, H. (2004): *Role of the gelatinous layer on the origin of the physical properties of the tension wood*. Journal of Wood Science. 50: 197-208.
12. Fang, C.H., B. Clair, J. Gril and S.Q. Liu (2008): *Growth stresses are highly controlled by the amount of G-layer in poplar tension wood*. IAWA Journal. 29: 237-246.

13. Wilson, B. and R.R. Archer (1979) *Tree design – Some biological solutions to mechanical problems*. Bioscience 29: 293-298.
14. Yoshida, M., T. Okuda, and T. Okuyama (2000): *Tension wood and growth stress induced by artificial inclination in Liriodendron tulipifera Linn. And Prunus spachiana Kitamura f. ascendens Kitamura*. Annals of Forest Science. 57: 739-746.
15. Yamamoto, H., M. Yoshida and T. Okuyama (2002): *Growth stress controls negative gravitropism in woody plant stems*. Planta 216: 280-292.
16. Kubler, H. (1987) *Growth stresses in trees and related wood properties*. Forest Products Abstract. 10: 62-118.
17. Okuyama, T., J. Doldan, H. Yamamoto and T. Ona (2004): *Heart splitting at crosscutting of Eucalyptus grandis logs*. Journal of Wood Science. 50: 1-6.
18. Abe, K. and H. Yamamoto (2007): *The influence of boiling and drying treatments on the behaviors of tension wood with gelatinous layers in Zelkova serrata*. Journal of Wood Science. 53: 5-10.
19. Clair, B. and B. Thibaut (2001): *Shrinkage of the gelatinous layer of poplar and beech tension wood*. IAWA Journal. 22: 121-131.
20. Norberg, H. and H. Meier (1966): *Physical and chemical properties of the gelatinous layer in tension wood fibres of aspen (Populus tremula L.)*. Holzforschung 6: 174-178.
21. Panshin, A.J. and C. de Zeeuw (1971): Textbook of wood technology, 3rd edn. McGraw-Hill Book Company, New York.
22. Boyd, J.D. (1977): *Relationship between fiber morphology and shrinkage of wood*. Wood Science and Technology. 11: 3-22.
23. Clair, B., B. Thibaut and J. Sugiyama (2005a): *On the detachment of the gelatinous layer in tension wood fiber*. Journal of Wood Science. 51: 218-221.
24. Abe, K. and H. Yamamoto (2006): *Behavior of the cellulose microfibril in shrinking woods*. Journal of Wood Science. 52: 15-19.
25. Abe, K. and H. Yamamoto (2005): *Mechanical interaction between cellulose microfibril and matrix substance in wood cell wall determined by X-ray diffraction*. Journal of Wood Science. 51: 334-338.
26. Hengstenberg, J. and H. Mark (1928): *Rontgenuntersuchungen uber den Bau der C-Ketten in Kohlenwasserstoffen*. Zeitschrift fur Kristallographie. 67: 583.
27. Kollmann, F. and H. Krech (1960): *Dynamic measurement of Damping Capacity and elastic properties of wood*. Holz als Roh- und Werkstoff. 18: 41-54.
28. Kojima, Y. and H. Yamamoto (2004): *Properties of the cell wall constituents in relation to the longitudinal elasticity of wood – Part 2. Origin of the moisture dependency of the longitudinal elasticity of wood*. Wood Science and Technology. 37: 427-434.
29. Clair, B., Gril J, K. Baba, T. Thibaut and J. Sugiyama (2005b): *Precautions for the structural analysis of the gelatinous layer in tension wood*. IAWA Journal 26: 189-196.
30. Clair, B., J. Gril, F. Di Renzo, H. Yamamoto and F. Quignard (2008): *Characterization of a gel in the cell wall to elucidate the paradoxical shrinkage of tension wood*. Biomacromol 9, 494-498.
31. Nishikubo, N., T. Awano, A. Banasiak, V. Bouquin, F. Ibatullin, R. Funada, H. Brumer, T.T. Teeri, T. Hayashi, B. Sundberg and E.J. Mellerowicz (2007): *Xyloglucan end-transglycosylase (XET) functions in gelatinous layer of tension wood fiber in Poplar – A glimpse into the mechanism of the balancing act of trees*. Plant and Cell Physiology. 48: 843-855.
32. Fang, C.H., B. Clair, J. Gril and T. Almeras (2007): *Transverse shrinkage in G-fibers as the function of cell wall layering and growth strain*. Wood Science and Technology. 41: 659-671
33. Cousins, W.J. (1976): *Elastic modulus of lignin as related to moisture content*. Wood Science and Technology. 10: 9-17.
34. Cousins, W.J. (1978): *Young's modulus of hemicellulose as related to moisture content*. Wood Science and Technology. 12: 161-167.
35. Salmén, L. and A.M. Olsson (1998): *Interaction between hemicellulose, lignin and cellulose: Structure-property relationships*. Journal of Pulp and Paper Science. 24: 99-103.
36. Akerholm, M. and L. Salmén (2003): *The oriented structure of lignin and its viscoelastic properties studied by static and dynamic FT-IR spectroscopy*. Holzforschung 57: 459-465.